

Probing the Role of Active Site Residues in NikD, an Unusual Amino Acid Oxidase That Catalyzes an Aromatization Reaction Important in Nikkomycin Biosynthesis[†]

Phaneeswara-Rao Kommoju, Robert C. Bruckner, Patricia Ferreira, and Marilyn Schuman Jorns*

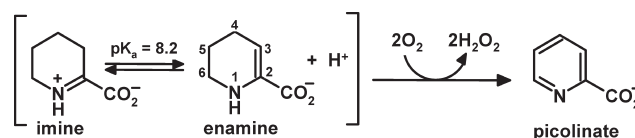
Department of Biochemistry and Molecular Biology, Drexel University College of Medicine, Philadelphia, Pennsylvania 19102

Received April 22, 2009; Revised Manuscript Received June 16, 2009

ABSTRACT: NikD catalyzes a remarkable aromatization reaction that converts piperideine 2-carboxylate (P2C) to picolinate, a key component of the nonribosomal peptide in nikkomycin antibiotics. The enzyme exhibits a FAD–Trp355 charge-transfer band at weakly alkaline pH that is abolished upon protonation of an unknown ionizable residue that exhibits a pK_a of 7.3. Stopped-flow studies of the reductive half-reaction with wild-type nikD and P2C show that the enzyme oxidizes the enamine tautomer of P2C but do not distinguish among several possible paths for the initial two-electron oxidation step. Replacement of Glu101 or Asp276 with a neutral residue does not eliminate the ionizable group, although the observed pK_a is 1 or 2 pH units higher, respectively, compared with that of wild-type nikD. Importantly, the mutations cause only a modest decrease (< 5-fold) in the observed rate of oxidation of P2C to dihydropicolinate. The results rule out the only possible candidates for a catalytic base in the initial two-electron oxidation step. This outcome provides compelling evidence that nikD oxidizes the bond between N(1) and C(6) in the enamine tautomer of P2C, ruling out alternative paths that require an active site base to mediate the oxidation of a carbon–carbon bond. Because the same restraint applies to the second two-electron oxidation step, the dihydropicolinate intermediate must be converted to an isomer that contains an oxidizable carbon–nitrogen bond. A novel role is proposed for reduced FAD as an acid–base catalyst in the isomerization of dihydropicolinate.

Nonribosomal peptides constitute an important group of natural products that display a broad range of useful therapeutic properties, including antifungal, antibacterial, immunosuppressive, and anticancer activities. The diversity of these natural products is achieved, in part, by the incorporation of a wide variety of nonproteogenic amino acids. Nikkomycins are potent antifungal agents that act by blocking the biosynthesis of chitin, the second most abundant polysaccharide in Nature (1, 2). The nonribosomal peptide moiety of nikkomycins features an N-terminal pyridyl residue, derived from L-lysine, that is essential for antibiotic activity. Synthesis of the pyridyl moiety requires a L-lysine α -aminotransferase (3) and nikD, an unusual amino acid oxidase that contains 1 mol of covalently bound FAD¹ (4) and acts as an obligate two-electron acceptor (5). The α -aminotransferase converts L-lysine to piperideine 2-carboxylate (P2C), a compound that can exist in imine and enamine tautomeric forms (6–8). NikD catalyzes a remarkable aromatization reaction that converts P2C to picolinate, accompanied by the reduction of 2 mol of oxygen to hydrogen peroxide (Scheme 1) (5).

Scheme 1: NikD-Catalyzed Four-Electron Oxidation of P2C to Picolinate



The first step in the nikD reaction involves formation of an enzyme·substrate charge-transfer complex with the electron-rich P2C enamine. The ES complex is converted into a reduced enzyme·dihydropicolinate (DHP) complex in a second step that exhibits a hyperbolic dependence on substrate concentration (9). There are several possible paths for this initial two-electron oxidation step (Scheme 2). Oxidation of the bond between N(1) and C(6) in the enamine tautomer (Scheme 2, path A) is consistent with results obtained in structural and biochemical studies (4, 10). In addition, nikD exhibits homology with monomeric sarcosine oxidase (MSOX) and other members of a flavoenzyme family that oxidize carbon–nitrogen bonds in various amino acid substrates (11–16). The available data do not, however, provide definitive evidence to rule out alternate reaction paths, such as oxidation of a carbon–carbon bond between C(4) and C(5) or C(5) and C(6) in the enamine (Scheme 2, path B or C, respectively).

The product of the initial two-electron oxidation step, a reduced enzyme·DHP complex, reacts with oxygen to produce

[†]This work was supported in part by Grant AI 55590 (M.S.J.) from the National Institutes of Health.

*To whom correspondence should be addressed. Phone: (215) 762-7495. Fax: (215) 762-4452. E-mail: marilyn.jorns@drexelmed.edu.

Abbreviations: FAD, flavin adenine dinucleotide; P2C, piperideine 2-carboxylate; CHA, 1-cyclohexenoate; MeSeA, methylselenoacetate; KIE, kinetic isotope effect; ES complex, enzyme·substrate complex; MSOX, monomeric sarcosine oxidase; DHP, dihydropicolinate; PDB, Protein Data Bank.

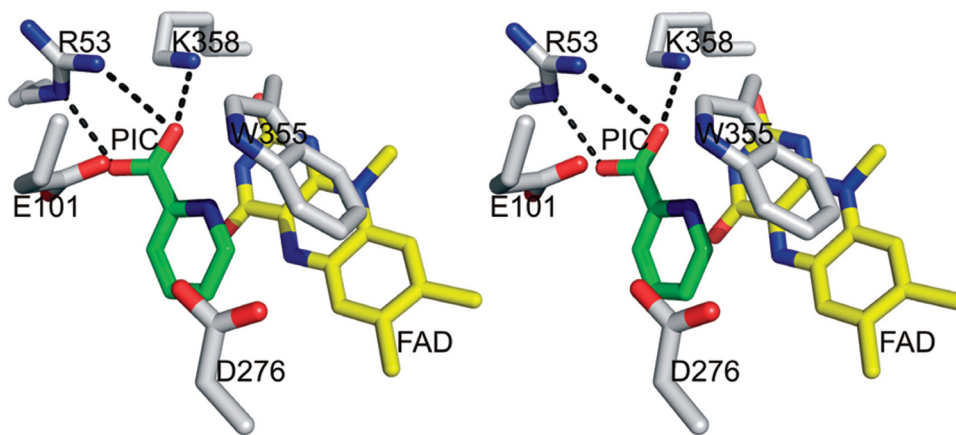
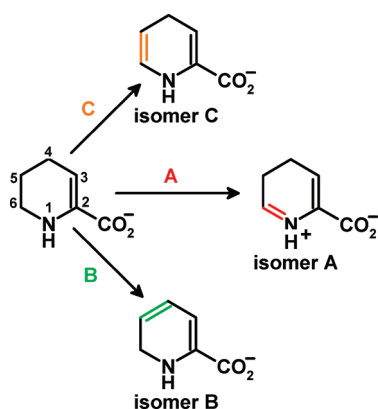


FIGURE 1: Stereoview of the *nikD* active site in the closed form (PDB entry 2OLN). Carbons are colored yellow in FAD, green in picolinate (PIC), and white in amino acid residues. Oxygen and nitrogen atoms are colored red and blue, respectively, in all structures. Hydrogen bonds are represented by dashed lines.

Scheme 2: Possible Paths for the Two-Electron Oxidation of the Enamine Tautomer of P2C to Isomeric Dihydropicolinates



hydrogen peroxide and an oxidized enzyme·DHP complex that can undergo a second redox cycle. It has been suggested that the second redox cycle may require prior conversion of the initially formed DHP intermediate to another isomer that can be oxidized to picolinate in a reaction that does not involve a change in regioselectivity as compared with the first redox cycle (9).

The active site in *nikD* is located at the interface between flavin- and substrate-binding domains. Crystal structures have been determined for two forms of a complex of the wild-type enzyme with picolinate (10). In the closed form, the active site is inaccessible to solvent. Picolinate is bound close to and parallel with the flavin ring, whereas the indole ring of Trp355 is perpendicular to the flavin ring (Figure 1). The ligand binding mode in this form is compatible with redox catalysis and resembles that observed with ligand-bound forms of MSOX. In the open form, the active site in *nikD* is accessible to solvent. However, the picolinate ligand and Trp355 have reoriented in the open form so that picolinate is perpendicular to the flavin and the indole ring of Trp355 is stacked atop the flavin ring.

Solutions of ligand-free *nikD* at weakly alkaline pH exhibit two typical flavin absorption maxima at >300 nm and an unusual long-wavelength absorption band due to charge-transfer interaction between FAD and Trp355 (17). The charge-transfer interaction requires a coplanar configuration of the flavin and indole rings, as observed in the crystal structure of the open form of the enzyme·picolinate complex. A long-wavelength absorption band is not observed with solutions of free *nikD* at weakly

acidic pH because of protonation of an unknown residue that exhibits a pK_a of 7.3 (4). The results suggest that, depending on pH, the side chain of Trp355 in solutions of free *nikD* may assume either of the conformations observed in the two crystal forms. However, the closed form of the enzyme·picolinate complex is likely to be the major species present in solutions of this complex, as judged by the absence of a charge-transfer band even at weakly alkaline pH.

Flavin-dependent oxidation of carbon–nitrogen or carbon–carbon bonds has been shown to involve transfer of hydride from substrate CH to flavin N(5) (18, 19). An active site base is required for oxidation of carbon–carbon bonds because, prior to or concomitant with hydride transfer, a proton must be abstracted from the adjacent carbon (18, 20). An active site base is not, however, required for oxidation of carbon–nitrogen bonds. We reasoned that this feature might therefore permit at least partial discrimination among the several possible paths for the two-electron oxidation of the P2C enamine (Scheme 2). There are only four ionizable residues within a ~ 5 Å radius of the bound ligand in the closed form of the *nikD*·picolinate complex (Figure 1). The carboxylate of picolinate is hydrogen bonded to the side chains of Arg53 and Lys358, which are homologous to Arg52 and Lys348, respectively, in MSOX. Asp276 in *nikD* aligns with His269, a catalytically important residue in MSOX (21). Glu101 in *nikD* is part of a mobile hairpin loop (Asp94–Gly102) that blocks access to the active site in the closed form. There is no counterpart to this loop in MSOX. Although neither is optimally positioned, a possible role for Glu101 or Asp276 as a catalytic base cannot be ruled out on the basis of the observed crystal structure of the enzyme·product complex because the latter may exhibit conformational differences compared with the reactive enzyme·substrate charge-transfer complex.

In this paper, we investigate the effect of replacing Asp276 or Glu101 with a neutral residue on steady-state turnover and the reductive half-reaction with P2C. We have also examined the effect of these substitutions on the spectral properties of the mutant enzymes to determine whether Asp276 or Glu101 might correspond to the ionizable group that appears to modulate the conformation of the indole ring of Trp355 in wild-type *nikD*. The results provide compelling evidence in favor of one of the possible paths for the initial two-electron oxidation of P2C and place important constraints on the mechanism of the second two-electron oxidation step.

Table 1: Primers Used for Mutagenesis^a

primer type	forward	backward
external	START 5'-GACTCACTATAGGGAGACCACAACGGTTTCCCTCTAG-3'	END 5'-GTCGCCACCGTCGTCGGTTGAGTCGAAGGAAAGCCC-3'
internal	Asp276Asn 5'-GTGCGCTGCGGGCCGaatTCGAGGTGGAC-3' Glu101Gln 5'-GACGTCGTACCAACcAGGGCCAGATCTCGGGG-3'	5'-CACGCGACGCCCCGGCttaAAGCTCCACCTG-3' 5'-CTGCAGCAGTTGTTGgTCCCGGTCTAGAGCCCC-3'

^a Mutagenic sites in the primers are shown with lowercase letters; the codon targeted for mutagenesis is underlined.

EXPERIMENTAL PROCEDURES

Materials. Methylselenoacetate was a generous gift from L. Silks (National Stable Isotope Resource at Los Alamos, Los Alamos, NM). 1-Cyclohexenoate was obtained from Aldrich. P2C was prepared as described by Bruckner et al. (5). Restriction enzymes and T4 DNA ligase were purchased from New England Biolabs. *Pfu* DNA polymerase was obtained from Stratagene.

Mutation of Asp276 to Asn or Glu101 to Gln. Mutations were generated by using plasmid pDV101 (4) as a template and the overlap extension polymerase chain reaction (PCR) method described by Ho et al. (22). PCRs were conducted using a Hybaid Touchdown Thermocycler or a Perkin-Elmer 9600 GeneAmp PCR System, and products were purified as previously described (17). The left-hand fragment was generated using START (external primer) as the forward primer and an internal backward primer containing the desired mutation (see Table 1). The right-hand fragment was generated using an internal forward primer containing the desired mutation and END (external primer) as the backward primer. The purified left- and right-hand fragments were combined using START and END as forward and backward primers, respectively. The final PCR product was purified, digested with *NdeI* and *XhoI*, purified again, and then subcloned between the *NdeI* and *XhoI* sites of plasmid pET23a. The resulting construct was used to transform *Escherichia coli* BL21(DE3) cells to ampicillin resistance. For screening, plasmid DNA was isolated from randomly selected clones and digested with *NdeI* and *XhoI*. Plasmids that exhibited the expected insert size (D276N pGPZ19 and E101Q pGPZ19 for the Asp276Asn and Glu101Gln mutations, respectively) were isolated and sequenced across the entire insert. Sequencing was conducted by MWG Biotech.

Enzyme Isolation. Recombinant wild-type nikD or Trp355-Phe was isolated from cells grown in Terrific Broth, as previously described (4, 17). The same procedure was used for expression and purification of Asp276Asn or Glu101Gln.

Steady-State Kinetic Studies. Steady-state kinetic studies with Asp276Asn or Glu101Gln were conducted by monitoring picolinate formation at 264 nm ($\epsilon = 3980 \text{ M}^{-1} \text{ cm}^{-1}$) (5) in 100 mM potassium phosphate buffer (pH 8.0) equilibrated at 25 °C with water-saturated gas mixtures containing 10, 21, 44, or 100% oxygen (balance nitrogen), as previously described (9). Steady-state kinetic parameters were estimated by fitting an equation for a sequential (eq 1) or ping-pong (eq 2) mechanism to data obtained with Asp276Asn or Glu101Gln, respectively (A is P2C; B is O₂).

$$v = \frac{V_{\max}[A][B]}{K_{ia}K_b + K_a[B] + K_b[A] + [A][B]} \quad (1)$$

$$v = \frac{V_{\max}[A][B]}{K_a[B] + K_b[A] + [A][B]} \quad (2)$$

Table 2: Spectral Properties of Asp276Asn, Glu101Gln, or Wild-Type NikD^a

	wild-type	Asp276Asn	Glu101Gln
λ_{\max} (nm)	379, 456	378, 456	373, 456
ϵ_{350} (M ⁻¹ cm ⁻¹)	1240	610	740
ϵ_{456} (M ⁻¹ cm ⁻¹)	11200 ^b	11900	10400
A_{280}/A_{456}	8.77–13.0 ^c	8.0	8.3
mol of FAD/mol of protein	0.54–0.90 ^c	0.93	1.1

^a Spectral properties were determined in 100 mM potassium phosphate buffer (pH 8.0) at 25 °C. ^b Data previously reported (4). ^c Data previously reported (17).

Steady-State Spectroscopy. Absorption spectra were recorded using an Agilent Technologies 8453 diode array spectrometer. All spectra are corrected for dilution. The concentration of the mutant or wild-type enzyme was determined at pH 8.0 on the basis of its absorbance at 456 nm and the extinction coefficients listed in Table 2. Extinction coefficients and the stoichiometry of covalent flavin incorporation were determined after denaturation of the mutant enzymes with 3 M guanidine hydrochloride, as previously described (15). Dissociation constants for complexes formed with the mutant enzymes and methylselenoacetate were determined by fitting a standard binding curve [$\Delta A_{\text{obs}} = \Delta A_{\text{max}}[\text{ligand}]/(K_d + [\text{ligand}])$] to the data. Titration data with picolinate or 1-cyclohexenoate were analyzed by using an equation for a tight binding inhibitor (eq 3)

$$\Delta A_{\text{obs}} = \frac{\Delta A_{\text{max}}}{2E_T} \left[X_T + E_T + K_d - \sqrt{(X_T + E_T + K_d)^2 - 4E_T X_T} \right] \quad (3)$$

where X_T and E_T are total ligand and enzyme concentrations, respectively. Spectra corresponding to 100% complex formation with methylselenoacetate, picolinate, or 1-cyclohexenoate were calculated as previously described (23). pH titrations with wild-type or mutant nikD were conducted as detailed in the legends of Figure 5 or 6, respectively. pK_a values were determined by fitting a theoretical pH titration curve [$y = (A[\text{H}^+] + BK_a)/([\text{H}^+] + K_a)$] to the data. Fitting of binding or pH titration equations was conducted by using Sigma Plot 10 (Systat Software).

Rapid Reaction Spectroscopy. Rapid reaction kinetic measurements were performed by using a Hi-Tech Scientific SF-61DX2 stopped-flow spectrometer. Data were collected in log mode to maximize the number of points acquired during the early phase of each reaction. All spectra or single-wavelength kinetic traces are the averages of at least three replicate shots. Reductive half-reactions with Asp276Asn or Glu101Gln and P2C were monitored by using diode array detection in anaerobic 100 mM potassium phosphate buffer (pH 8.0) containing 50 mM glucose

and glucose oxidase (14.7 units/mL). All components, except glucose oxidase, were placed in the main compartment of a tonometer. Glucose oxidase was tipped from a side arm into the main compartment after the solutions were made anaerobic by multiple cycles of evacuation, followed by flushing with oxygen-scrubbed argon. The entire flow circuit of the stopped-flow spectrometer was made anaerobic by an overnight incubation with anaerobic buffer containing 50 mM glucose and glucose oxidase (14.7 units/mL). All spectra are corrected for a small spectral contribution from P2C in the near-ultraviolet region. The kinetics of picolinate binding to Glu101Gln were monitored in aerobic 100 mM potassium phosphate buffer (pH 8.0) at 25 °C by using photomultiplier detection. Fitting of single-wavelength kinetic traces was conducted by using Sigma Plot 10 (Systat Software), KinetAsyst 3 (TgK Scientific), or Kinetic Studio (TgK Scientific).

RESULTS

Spectral Properties of Ligand-Free Asp276Asn and Glu101Gln. Wild-type *nikD* contains covalently bound FAD and exhibits two characteristic flavin absorption maxima at > 300 nm at pH 8.0 and an unusual long-wavelength absorption band due to charge-transfer interaction between FAD and Trp355. Although these general features are observed with Asp276Asn or Glu101Gln, the spectral properties of mutants and the wild-type enzyme exhibit certain distinct features. Thus, both mutants exhibit an ~50% decrease in the intensity of the long-wavelength absorption band. The Glu101Gln mutant displays a hypsochromic shift (6 nm) of the near-UV absorption maximum. The mutant and wild-type enzymes also exhibit differences in the extinction coefficient of the peak at 456 nm (Figure 2A and Table 2).

Does Mutation of Asp276 or Glu101 Affect the Binding of Substrate Analogues? Wild-type *nikD* forms spectrally similar complexes with various electron-poor analogues of P2C, such as picolinate, the product of the physiological reaction, or 1-cyclohexenoate (CHA), a 1-deaza analogue of the enamine tautomer of P2C. In each case, ligand binding at pH 8.0 eliminates the long-wavelength absorption band and increases the extinction coefficient of the band at 456 nm, accompanied by an enhancement of its vibronic resolution (4). Unlike the free enzymes, complexes formed by Asp276Asn or Glu101Gln with picolinate or CHA exhibit absorption spectra that are remarkably similar to those observed with wild-type *nikD*, as illustrated by results obtained with picolinate (Figure 2B). As one can see in the corresponding difference spectra (Figure 2B, inset), this outcome reflects differences in the nature of the ligand-induced perturbation that effectively counterbalance the spectral differences observed with the ligand-free enzymes.

Unlike picolinate or CHA, methylselenoacetate (MeSeA) is an electron-rich analogue of the reactive center in the enamine tautomer of P2C and forms a charge-transfer complex with wild-type *nikD* (9). A charge-transfer complex is also formed with the mutant enzymes, as judged by the diagnostic increase in absorption in the long-wavelength region observed upon titration with MeSeA (data not shown; see Figure S1 of the Supporting Information). The mutant charge-transfer bands are, however, shifted to higher energies compared with that of the wild-type enzyme, as estimated by the position of peaks observed in the corresponding difference spectra ($\lambda_{\text{max}} = 512, 530, \text{ or } 581 \text{ nm}$ with Asp276Asn, Glu101Gln, or wild-type *nikD*, respectively)

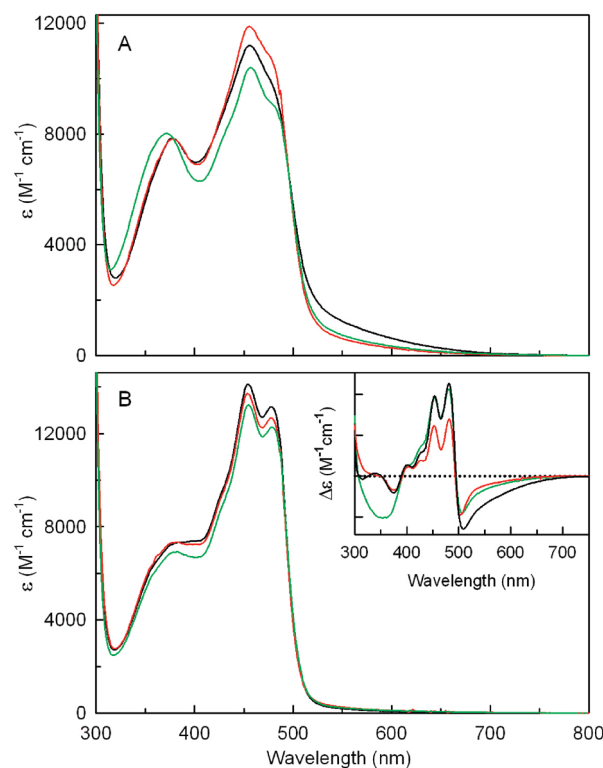


FIGURE 2: Spectral properties of free wild-type *nikD*, Asp276Asn, or Glu101Gln and the corresponding picolinate complexes. All spectra were recorded in 100 mM potassium phosphate buffer (pH 8.0) at 25 °C. In each panel or inset, spectra obtained with wild-type *nikD*, Asp276Asn, or Glu101Gln are colored black, red, or green, respectively. Panel A shows spectra obtained with the ligand-free enzymes. Panel B shows spectra calculated for 100% picolinate complex formation using data obtained in spectral titrations, as detailed in Experimental Procedures. The inset shows difference spectra obtained by subtracting the spectrum of the free enzyme from the spectrum calculated for 100% complex formation.

(Figure 3A). The observed increase in charge-transfer band energy suggests that the mutations may cause a decrease in flavin reduction potential. The mutant enzymes, especially Glu101Gln, appear to exhibit more intense charge-transfer bands than wild-type *nikD*, as estimated by the amplitude of charge-transfer peaks observed in difference spectra (Figure 3A). This feature is not, however, apparent in the absolute spectrum of the Asp276Asn complex, as judged by its lower absorption in the long-wavelength region ($\lambda > 550 \text{ nm}$) (Figure 3B). This difference arises because the hypsochromically shifted mutant charge-transfer band is partially obscured in the absolute spectrum by the red edge of the flavin absorption band.

Overall, the Asp276Asn mutation results in only minor changes in the stability of complexes formed with picolinate, CHA, or MeSeA, as judged by comparison of dissociation constants obtained with the mutant or wild-type enzyme. The complexes formed with the Glu101Gln mutant tend, however, to be more stable (2–14-fold) than the corresponding wild-type complexes (Table 3).

Spectrally Detectable Ionizable Groups in Wild-Type *NikD* or Trp355Phe. Solutions of ligand-free wild-type *NikD* do not exhibit a FAD–Trp355 charge-transfer band at weakly acidic pH. Increasing the pH from 6.3 to 9.0 at 10 °C results in the recovery of the charge-transfer band, accompanied by a decrease in absorbance at 456 nm (Figure 4A). Analysis of the increase in the long-wavelength absorbance at 550 nm as a

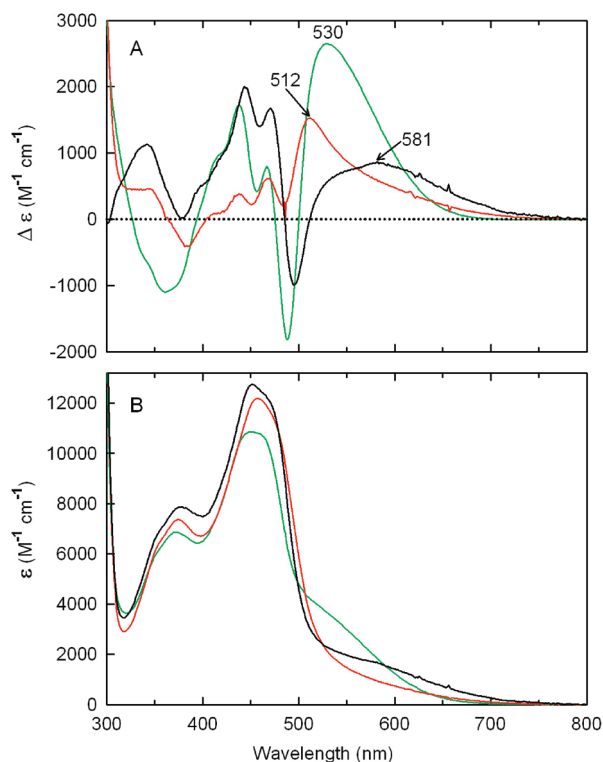


FIGURE 3: Comparison of difference (A) or absolute (B) spectra calculated for 100% complex formation with methylselenoacetate (MeSeA) and wild-type nikD (black curve), Asp276Asn (red curve), or Glu101Gln (green curve). The data for wild-type nikD were taken from ref 9.

Table 3: Properties of Complexes Formed with Wild-Type or Mutant NikD and Various Substrate Analogues^a

	wild-type ^b	Asp276Asn	Glu101Gln
picolinate			
K_d (μ M)	290 ± 40	420 ± 20	151 ± 2
1-cyclohexenoate			
K_d (μ M)	12.8 ± 0.9	6.5 ± 0.9	0.9 ± 0.1
methylselenoacetate			
K_d (mM)	1.07 ± 0.04	1.00 ± 0.03	0.112 ± 0.003
λ_{\max} (CT band) (nm)	581	512	530

^a Dissociation constants were determined on the basis of absorbance changes observed in spectral titrations conducted in 100 mM potassium phosphate buffer (pH 8.0) at 25 °C. ^b Data previously reported (9).

function of pH provides evidence for a single ionizable group with a pK_a of 7.31 ± 0.01 (Figure 4B). The observed pK_a is in excellent agreement with a value obtained in previous studies ($pK_a = 7.3$) that were conducted at 25 °C within a relatively narrow pH range (6.5–8.6) (4).

The lower temperature used in these studies extended the accessible pH range up to pH 11. Increasing the pH from 9.0 to 11.0 results in a loss of long-wavelength absorption, a decrease in absorbance at 456 nm, and a pronounced hypsochromic shift of the near-UV band from 375 to 362 nm, accompanied by an increase in absorbance at 350 nm (Figure 4A). Similar values for the spectral pK_a are obtained upon analysis of the absorbance decrease at 550 nm or the absorbance increase at 350 nm ($pK_a = 9.8 \pm 0.1$ or 9.75 ± 0.06 , respectively) (Figure 4B). The observed spectral changes are fully reversible upon acidification and, except for the long-wavelength region, are strikingly similar to

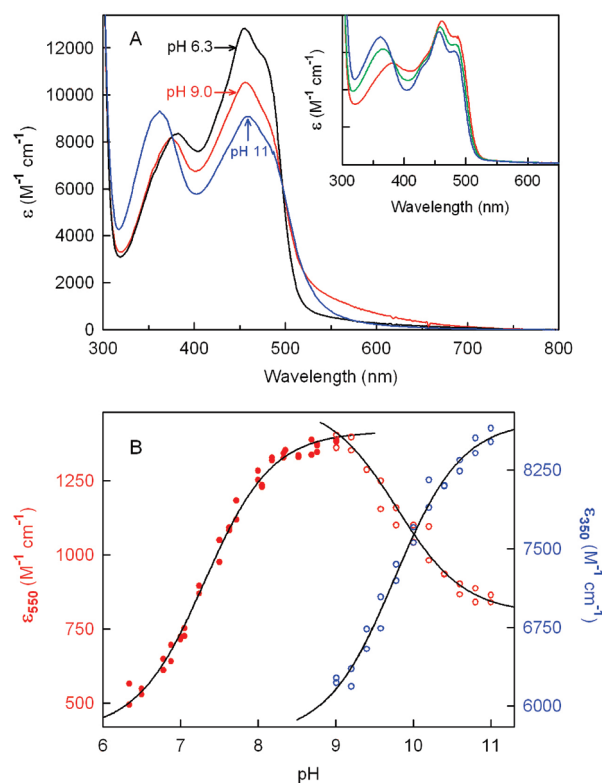


FIGURE 4: Effect of pH on the absorption spectrum of wild-type nikD or Trp355Phe. All spectra are averages of duplicate dilutions of a concentrated stock enzyme solution into 100 mM potassium phosphate (pH 6.34–8.05), potassium pyrophosphate (pH 8.05–9.58), or sodium carbonate (pH 9.78–11.0) buffer at 10 °C. Data in the pH range from pH 6.34 to 9.01 or from pH 9.01 to 11.0 with wild-type nikD were collected in two separate experiments and normalized to the same enzyme concentration. (A) Absorption spectra of wild-type nikD at pH 6.34, 9.01, and 11.0 are colored black, red, and blue, respectively. The inset shows absorption spectra of Trp355Phe at pH 8.02, 9.40, and 10.4 colored red, green, and blue, respectively. (B) The filled and empty red circles show extinction changes at 550 nm in the pH ranges from 6.34 to 9.01 and from 9.01 to 11.0, respectively. The empty blue circles show extinction changes at 350 nm in the pH range from 9.01 to 11.0. The solid black lines were obtained by fitting a theoretical pH titration curve [$y = (A[H^+] + BK_a)/([H^+] + K_a)$] to each data set, where y is the observed extinction and A and B are calculated extinction values at low and high pH, respectively.

those observed upon ionization at the N(3)H position of free FAD ($pK_a = 10.4$) (24).

Mutation of Trp355 to Phe eliminates the long-wavelength absorption band observed with wild-type nikD at slightly alkaline pH (17). Significantly, titration of Trp355Phe from pH 8.0 to 10.4 results in spectral changes that are fully characteristic of FAD ionization at the N(3)H group ($pK_a = 9.15 \pm 0.05$) (Figure 4A, inset). The results indicate that the FAD–Trp355 charge-transfer band observed with wild-type nikD at slightly alkaline pH is eliminated at higher pH values because of ionization at the N(3)H group in FAD or at acidic pH due to protonation of an unknown amino acid residue. It is worth noting that protonation of both groups results in an enormous (40%) increase in the extinction coefficient at 456 nm, as can be seen by comparison of spectra observed with the wild-type enzyme at pH 6.3 and 11.0 (Figure 4A).

Are the Ionizable Groups Observed with Wild-Type NikD Affected by Mutation of Glu101 or Asp276? Solutions of ligand-free Glu101Gln at pH 6.3 exhibit negligible absorbance in the long-wavelength region. Increasing the pH from 6.3 to 10.0

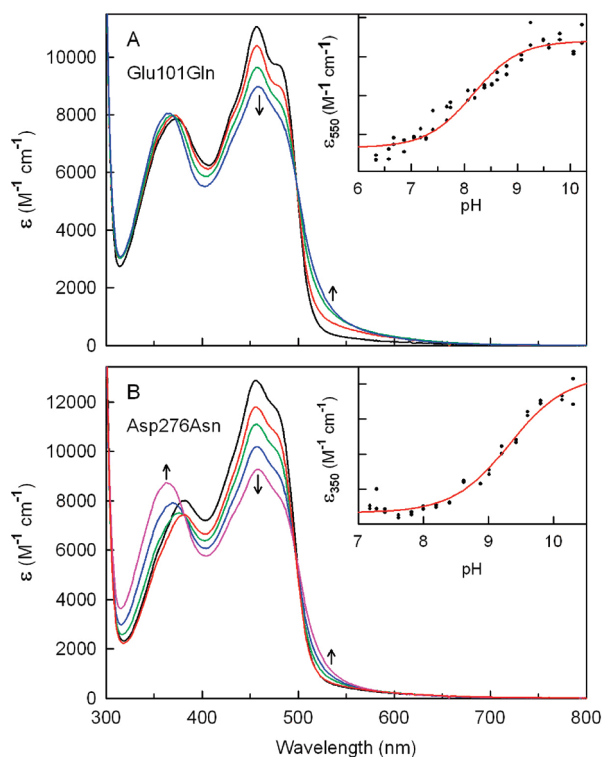


FIGURE 5: Effect of pH on the absorption spectrum of Glu101Gln or Asp276Asn. All spectra are averages of duplicate dilutions of concentrated stock solutions of the mutant enzymes into 100 mM potassium phosphate (pH 6.34–8.80), potassium pyrophosphate (pH 9.01–9.58), or sodium carbonate (pH 9.78–10.3) buffer at 10 °C. Arrows indicate the direction of the spectral changes observed with an increase in pH. (A) Absorption spectra of Glu101Gln at pH 6.34, 8.07, 9.08, and 10.06 are colored black, red, green, and blue, respectively. (B) Absorption spectra of Asp276Asn at pH 7.28, 7.62, 8.62, 9.42, and 10.30 are colored black, red, green, blue, and magenta, respectively. The inset in panel A or B shows a plot of extinction changes at 550 or 350 nm, respectively, as a function of pH. The solid black lines were obtained by fitting a theoretical pH titration curve [$y = (A[H^+] + BK_a)/([H^+] + K_a)$] to the data.

results in an increase in long-wavelength absorption, accompanied by a decrease in absorption at 456 nm (Figure 5A). The observed spectral change is strikingly similar to that observed upon ionization of a residue that exhibits a pK_a of 7.31 in wild-type nikD, as judged by comparison of the corresponding difference spectra (Figure 6A). Analysis of the absorbance increase observed with Glu101Gln at 550 nm as a function of pH provides evidence of a single ionizable group with a pK_a of 8.16 ± 0.07 (Figure 5A, inset). The results show that the pK_a is perturbed but not eliminated in the mutant, ruling out Glu101 as a possible candidate for the unknown ionizable residue in wild-type nikD. The effect of the Glu101Gln mutation on the ionization of the N(3)H group in FAD is unclear. A relatively small hypsochromic shift (7 nm) of the near-UV band is observed at pH > 8, but spectral changes characteristic of flavin ionization are not apparent at pH ≤ 10 , the upper pH limit accessible with this mutant.

Titration of Asp276Asn in the pH range from 7.3 to 10.3 results in a modest increase in absorbance at > 500 nm, an enormous decrease (30%) in absorbance at 456 nm, and a pronounced hypsochromic shift (20 nm) of the near-UV band, accompanied by a substantial increase in absorbance at 350 nm (Figure 5B). The overall spectral change is not cleanly isosbestic. Nevertheless, results obtained upon analysis of absorbance

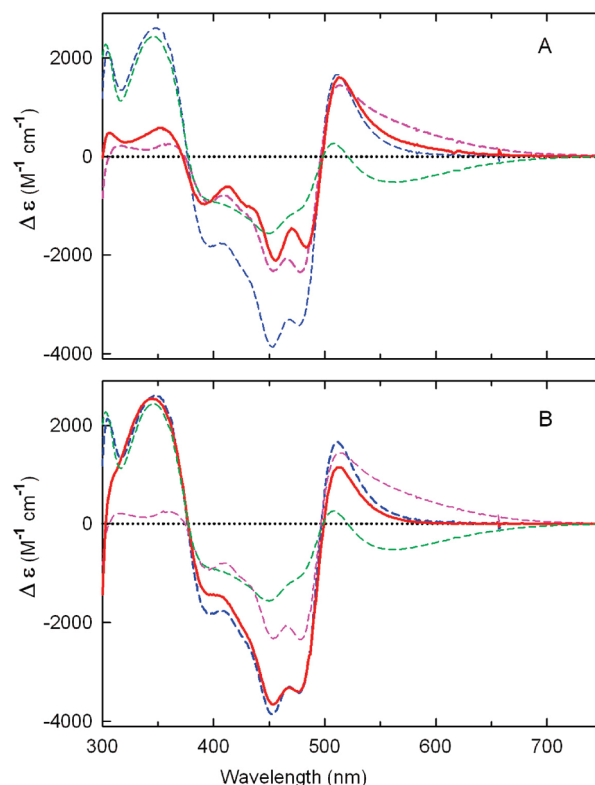


FIGURE 6: Comparison of difference spectra obtained for pH-dependent absorbance changes observed with Glu101Gln (A) or Asp276Asn (B) with those observed with wild-type nikD. (A) The solid red line was obtained by subtracting the spectrum observed with Glu101Gln at pH 6.34 from that observed at pH 10.06. (B) The solid red line was obtained by subtracting the spectrum observed with Asp276Asn at pH 7.28 from that observed at pH 10.3. Results obtained with wild-type nikD are indicated by the dashed spectra in each panel. The dashed magenta and blue curves were generated by subtracting the spectrum observed at pH 6.34 from spectra obtained at pH 9.01 and 11.0, respectively. The dashed green curve was generated by subtracting the spectrum observed at pH 9.01 from that observed at pH 11.0.

changes observed at four different wavelengths (550, 510, 453, or 350 nm) are consistent with the presence of a single ionizable group that exhibits a pK_a between 8.9 and 9.3 (Figure 5B, inset, and Table 4). On the other hand, difference spectra show that the overall spectral change observed with the mutant is remarkably similar to that observed with wild-type nikD when the pH is increased from 6.3 to 11.0 (Figure 6B). Importantly, the latter pH shift results in the ionization of two groups in wild-type nikD, an unknown residue and FAD. The results strongly suggest that the pH-dependent spectral changes observed with Asp276Asn reflect ionization of the same two groups. Unlike wild-type nikD, the two groups are likely to exhibit very similar pK_a values in Asp276Asn, a scenario consistent with the titration behavior observed with this mutant.

Effect of Changing Asp276 to Asn on Turnover and the Kinetics of the Reductive Half-Reaction with P2C. Turnover rates with P2C and oxygen were measured at pH 8.0 by monitoring picolinate formation at 264 nm (5). Double-reciprocal plots of reaction rate versus P2C concentration at different oxygen concentrations or versus oxygen concentration at different P2C concentrations are linear and intersect to the left of the y-axis, just below the x-axis (data not shown; see Figure S2 of the Supporting Information), as observed with wild-type nikD at pH 8.0 (9). The results are consistent with a sequential mechanism in

Table 4: Spectrally Detectable Ionizable Groups in Wild-Type NikD or Active Site Mutants^a

	wild-type		Trp355Phe		Asp276Asn		Glu101Gln	
	pK _a	λ (nm)	pK _a	λ (nm)	pK _a ^b	λ (nm)	pK _a	λ (nm)
pK _{a1}	7.31 ± 0.03 ^c	550	nd ^d		8.9 ± 0.1 9.29 ± 0.06 9.1 ± 0.1 9.32 ± 0.06	550 510 453 350	8.16 ± 0.07	550
pK _{a2}	9.8 ± 0.1 9.75 ± 0.06	550 350	9.15 ± 0.05	350				

^a Spectral pK_a values were determined at 10 °C on the basis of absorbance changes at the indicated wavelength, as detailed in the text and the legends of Figures 5 and 6. ^b The observed pK_a is likely to reflect an average value for two ionizable groups that exhibit very similar pK_a values, as discussed in the text. ^c A value of 7.3 was previously reported for pK_{a1} by Venci et al. (4). ^d Not detectable.

Scheme 3: A Minimal Steady-State Kinetic Mechanism for the NikD-Catalyzed Conversion of P2C to Picolinate (P)^a

^a The red box indicates the portion of the overall reaction that is monitored in reductive half-reaction studies.

which oxygen reacts with a reduced enzyme•DHP complex to yield an oxidized enzyme•DHP complex that can undergo a second redox cycle to produce picolinate (Scheme 3). The steady-state kinetic parameters listed in Table 5 were obtained by fitting an equation for a sequential mechanism (eq 1) to the data obtained with Asp276Asn.

The turnover rate observed with Asp276Asn at saturating concentrations of P2C and oxygen is ~2-fold slower than the rate observed with wild-type nikD. This outcome does not, however, preclude a catalytically important role for Asp276 in the oxidation of P2C to DHP because this step may not be rate-limiting during turnover, as observed with wild-type nikD (9). The effect of the Asp276Asn mutation on the kinetics of P2C oxidation to DHP was investigated by monitoring the anaerobic reduction of the mutant with various concentrations of P2C in a stopped-flow spectrophotometer. The reaction observed with 100 μM P2C exhibits an initial lag, followed by a decrease in absorbance at 456 nm. The lag becomes progressively smaller at higher P2C concentrations and is barely detectable at 2500 μM P2C (Figure 7A). A similar feature is observed with wild-type nikD and reflects the relatively slow formation of the enzyme•P2C complex (9).

The decrease in absorbance at 456 nm observed with Asp276Asn exhibits biphasic kinetics ($y = Ae^{-k_{\text{fast}}t} + Be^{-k_{\text{slow}}t} + C$) over the entire range of P2C concentrations. Approximately 85% of the total absorbance decrease occurs in a fast phase and is attributed to the formation of a reduced enzyme•DHP complex. The rate observed for the fast phase exhibits a hyperbolic dependence on the concentration of P2C [$k_{\text{obs}} = k_{\text{lim}}[\text{P2C}]/(K_{\text{d app}} + [\text{P2C}])$] (Figure 8A), as observed with wild-type nikD (9). The apparent second-order rate constant for the reaction of Asp276Asn with P2C, as estimated from stopped-flow data [$k_{\text{lim}}/K_{\text{d app}} = (1.01 \pm 0.01) \times 10^5 \text{ M}^{-1} \text{ s}^{-1}$], is in excellent agreement with a value calculated using steady-state kinetic parameters [$k_{\text{cat}}/K_{\text{m P2C}} = (0.9 \pm 0.1) \times 10^5 \text{ M}^{-1} \text{ s}^{-1}$] (Table 5). The limiting

rate observed with Asp276Asn at saturating P2C ($k_{\text{lim}} = 11.1 \pm 0.2 \text{ s}^{-1}$) is ~10-fold faster than the observed turnover rate ($k_{\text{cat}} = 1.22 \pm 0.04 \text{ s}^{-1}$) and ~5-fold slower than the limiting rate observed with wild-type nikD ($k_{\text{lim}} = 53 \pm 1 \text{ s}^{-1}$). The modest effect of the Asp276Asn mutation on the limiting rate of the fast phase rules out a role for Asp276 as a critical active site base in the oxidation of P2C to DHP.

The rate observed with Asp276Asn for the slow phase of the reductive half-reaction is independent of the concentration of P2C ($k_{\text{slow}} = 3.0 \pm 0.3 \text{ s}^{-1}$), at least partially rate-limiting during turnover ($k_{\text{cat}} = 1.22 \pm 0.04 \text{ s}^{-1}$), and, within experimental error, identical to the rate obtained for the corresponding step with wild-type nikD ($k_{\text{slow}} = 2.7 \pm 0.1 \text{ s}^{-1}$). Our previous studies with wild-type nikD indicate that the slow step is likely to involve isomerization of an initially formed reduced enzyme•DHP complex (9).

Effect of the Glu101Gln Mutation on Turnover and the Kinetics of the Reductive Half-Reaction with P2C. Double-reciprocal plots obtained for the aerobic turnover of Glu101Gln with P2C at pH 8.0 exhibit parallel lines (data not shown; see Figure S3 of the Supporting Information), in contrast to the intersecting pattern observed with wild-type nikD at this pH. The results indicate that an irreversible step occurs prior to reaction of the reduced mutant enzyme with oxygen, which will be discussed. The steady-state kinetic parameters listed in Table 5 were obtained by fitting an equation for a ping-pong mechanism (eq 2) to the data obtained with Glu101Gln.

The turnover rate observed with Glu101Gln at saturating concentrations of P2C and oxygen is ~5-fold slower than the rate observed with wild-type nikD. To directly assess the effect of the Glu101Gln mutation on the rate of oxidation of P2C to DHP, we investigated the kinetics of the reductive half-reaction over a wide range of P2C concentrations (from 100 to 10000 μM). A lag is not observed when the reduction of Glu101Gln is monitored at 456 nm at any substrate concentration tested, whereas a very slow, small increase in absorbance is observed at the end of the reaction, unlike results obtained with wild-type nikD or Asp276Asn.

The decrease in absorbance at 456 nm observed with Glu101Gln exhibits biphasic kinetics ($y = Ae^{-k_{\text{very fast}}t} + Be^{-k_{\text{fast}}t} + C$) (Figure 7B). Approximately 80% of the total absorbance decrease occurs in the fast phase and is attributed to the formation of a reduced enzyme•DHP complex. The rate observed for the fast phase exhibits a hyperbolic dependence on the concentration of P2C [$k_{\text{obs}} = k_{\text{lim}}[\text{P2C}]/(K_{\text{d app}} + [\text{P2C}])$] (Figure 8B), as observed with wild-type nikD (9). The apparent second-order rate constant for the reaction of Glu101Gln with P2C, as estimated from stopped-flow data [$k_{\text{lim}}/K_{\text{d app}} = (9 \pm 1) \times 10^3 \text{ M}^{-1} \text{ s}^{-1}$], is in fairly good agreement with a value

Table 5: Kinetic Parameters for the Reaction of Wild-Type or Mutant NikD with P2C at pH 8.0 and 25 °C

enzyme	reductive half-reaction ^a				steady-state turnover ^b		
	k_{lim} (s ⁻¹)	k_{slow} (s ⁻¹)	$K_{\text{d app}}$ (μM)	$k_{\text{lim}}/K_{\text{d app}}$ (M ⁻¹ s ⁻¹)	k_{cat} (s ⁻¹)	$k_{\text{cat}}/K_{\text{m P2C}}$ (M ⁻¹ s ⁻¹)	$k_{\text{cat}}/K_{\text{m O}_2}$ (M ⁻¹ s ⁻¹)
wild-type	53 ± 1	2.7 ± 0.1	260 ± 20	(2.0 ± 0.2) × 10 ⁵	2.3 ± 0.2	(2.0 ± 0.3) × 10 ⁵	(2.6 ± 0.2) × 10 ³
Asp276Asn	11.1 ± 0.2	3.0 ± 0.3	110 ± 10	(1.01 ± 0.09) × 10 ⁵	1.22 ± 0.04	(0.9 ± 0.1) × 10 ⁵	(2.0 ± 0.2) × 10 ³
Glu101Gln	13.9 ± 0.9	—	1400 ± 200	(9 ± 1) × 10 ³	0.50 ± 0.01	(4.9 ± 0.2) × 10 ³	(1.25 ± 0.07) × 10 ³

^a A biphasic decrease in absorbance at 456 nm is observed with wild-type nikD, Asp276Asn, or Glu101Gln. All three preparations exhibit a rapid phase (k_{fast}) that comprises most of the observed absorbance change and exhibits a hyperbolic dependence on the concentration of P2C [$k_{\text{obs}} = k_{\text{lim}}[\text{P2C}]/(K_{\text{d app}} + [\text{P2C}])$]. With wild-type nikD and Asp276Asn, the rapid phase is followed by a slow phase (k_{slow}) that is independent of the concentration of P2C. With Glu101Gln, the rapid phase is preceded by a very fast phase ($k_{\text{very fast}}$) that exhibits a linear dependence on the concentration of P2C [slope = $(8.8 \pm 0.2) \times 10^3 \text{ M}^{-1} \text{ s}^{-1}$; y-intercept = $10.1 \pm 0.9 \text{ s}^{-1}$]. The biphasic absorbance decrease at 456 nm is preceded by an initial lag phase (wild-type nikD or Asp276Asn) or followed by a very slow absorbance increase (Glu101Gln), as described in the text. ^b Double-reciprocal plots obtained with wild-type nikD or Asp276Asn exhibit intersecting lines ($K_{\text{i P2C}} = 2.9 \pm 0.8$ or $8 \pm 2 \text{ μM}$, respectively). The corresponding plots with Glu101Gln exhibit parallel lines.

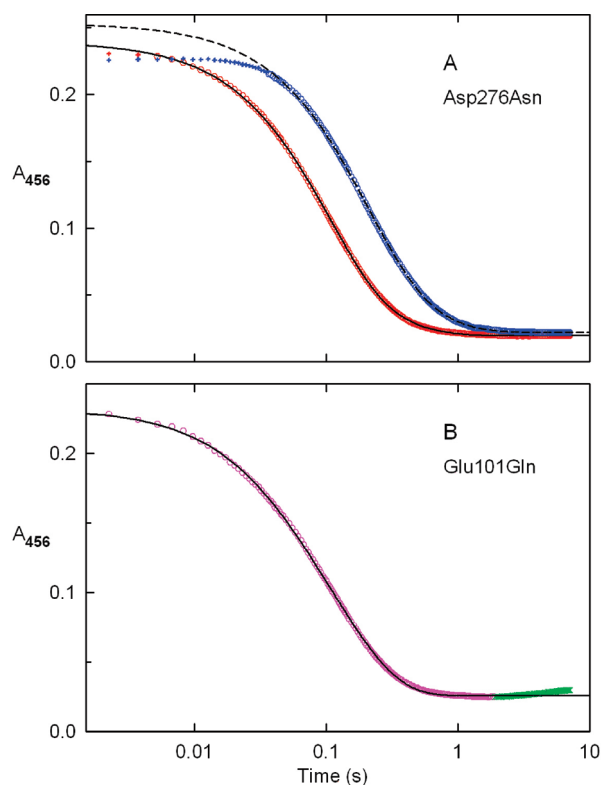


FIGURE 7: Kinetics of the anaerobic reduction of Asp276Asn (A) or Glu101Gln (B) with P2C. Reactions were conducted at 25 °C in 100 mM potassium phosphate buffer (pH 8.0) containing 50 mM glucose and 14.7 units/mL glucose oxidase. (A) The solid black line was obtained by fitting a double-exponential equation ($y = Ae^{-k_{\text{fast}}t} + Be^{-k_{\text{slow}}t} + C$) to absorbance changes observed for the reaction of Asp276Asn with 2500 μM P2C (empty red circles). The dashed black line is the corresponding fit obtained for reaction of Asp276Asn with 100 μM P2C (empty blue circles). Data points in the initial lag phases (red or blue pluses) were not used in fitting. (B) The black line was obtained by fitting a double-exponential equation ($y = Ae^{-k_{\text{fast}}t} + Be^{-k_{\text{slow}}t} + C$) to absorbance changes observed for the reaction of Glu101Gln with 1500 μM P2C (empty magenta circles). A slow small increase in absorbance at 456 nm observed at longer times (green) was not used in the fitting.

calculated using steady-state kinetic parameters [$k_{\text{cat}}/K_{\text{m P2C}} = (4.9 \pm 0.2) \times 10^3 \text{ M}^{-1} \text{ s}^{-1}$] (Table 5). The limiting rate observed with Glu101Gln at saturating P2C ($k_{\text{lim}} = 13.9 \pm 0.9 \text{ s}^{-1}$) is ~30-fold faster than the observed turnover rate ($k_{\text{cat}} = 0.50 \pm 0.01 \text{ s}^{-1}$) and ~4-fold slower than the limiting rate observed with

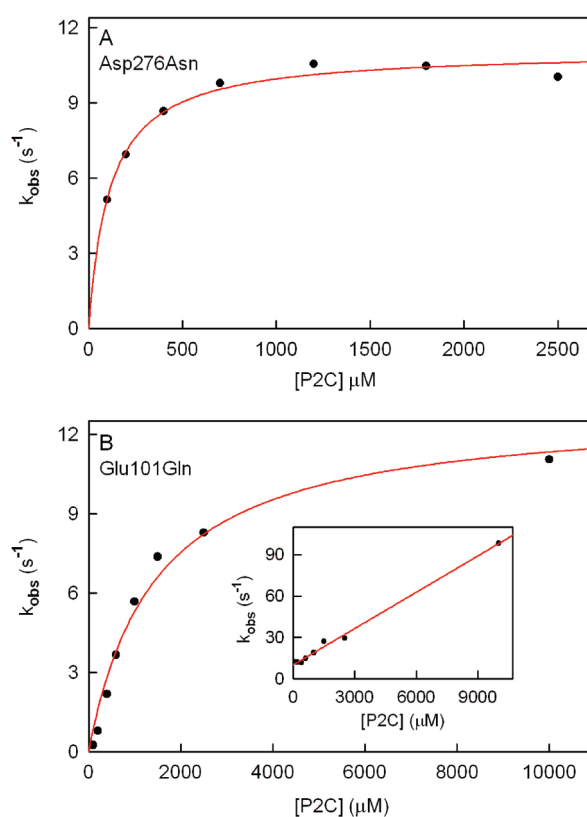


FIGURE 8: Dependence of rate constants observed for the anaerobic reduction of Asp276Asn (A) or Glu101Gln (B) on the concentration of P2C. Reactions were conducted at 25 °C in 100 mM potassium phosphate buffer (pH 8.0) containing 50 mM glucose and 14.7 units/mL glucose oxidase. Panels A and B show plots of rate constants observed for the fast phase of the anaerobic reduction of Asp276Asn and Glu101Gln, respectively. The solid red line in each panel was obtained by fitting a hyperbolic equation [$k_{\text{obs}} = k_{\text{lim}}[\text{P2C}]/(K_{\text{d app}} + [\text{P2C}])$] to the data (black circles). The inset in panel B is a plot of rate constants observed for the very fast phase of the anaerobic half-reaction with Glu101Gln. The red line is a linear regression analysis of the data [slope = $(8.8 \pm 0.2) \times 10^3 \text{ M}^{-1} \text{ s}^{-1}$; y-intercept = $10.1 \pm 0.9 \text{ s}^{-1}$; $r^2 = 0.9955$].

wild-type nikD ($k_{\text{lim}} = 53 \pm 1 \text{ s}^{-1}$). The small effect of the Glu101Gln mutation on the limiting rate of the fast phase rules out a possible role for Glu101 as a catalytic base in the oxidation of P2C to DHP.

With the Glu101Gln mutant, the fast phase is preceded by a very fast phase ($k_{\text{very fast}}$) that exhibits a linear dependence on the

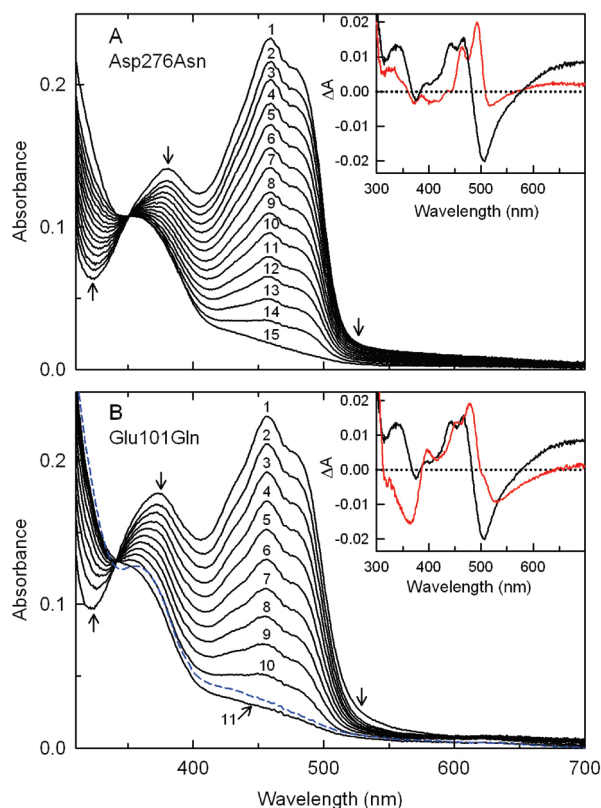


FIGURE 9: Spectral course of the anaerobic reduction of Asp276Asn (A) or Glu101Gln (B) with P2C. Reactions were conducted at 25 °C in 100 mM potassium phosphate buffer (pH 8.0) containing 50 mM glucose and 14.7 units/mL glucose oxidase. (A) Curves 1–15 were recorded 0.00224, 0.0142, 0.0217, 0.0322, 0.0427, 0.0555, 0.0675, 0.0855, 0.1035, 0.1245, 0.1560, 0.1920, 0.2520, 0.3630, and 7.125 s, respectively, after 18.5 μ M Asp276Asn was mixed with 2500 μ M P2C. Arrows indicate the direction of the observed spectral changes. In the inset, the red curve is the difference spectrum obtained when the absorption spectrum of free Asp276Asn was subtracted from the spectrum observed 0.74 ms after the enzyme was mixed with 2500 μ M P2C. The black curve is the corresponding difference spectrum obtained for the reaction of 18.6 μ M wild-type nikD with 2500 μ M P2C. (B) Curves 1–11 (solid black lines) show spectra recorded 0.00074, 0.0112, 0.0217, 0.0352, 0.0525, 0.0735, 0.1005, 0.1335, 0.1800, 0.2700, and 1.875 s, respectively, after 21.1 μ M Glu101Gln was mixed with 1500 μ M P2C. Arrows indicate the direction of the observed spectral changes during this portion of the reaction. The dashed blue curve was recorded 7.125 s after mixing. In the inset, the red curve is the difference spectrum obtained by subtracting the spectrum of free Glu101Gln from the spectrum observed 0.74 ms after the enzyme was mixed with 10000 μ M P2C. The black curve is the corresponding difference spectrum observed 0.74 ms after 18.6 μ M wild-type nikD was mixed with 2500 μ M P2C.

concentration of P2C and a finite y -intercept (Figure 8B, inset). The nature of the very rapid phase is unclear.

Spectral Properties of the ES Complex Formed with Asp276Asn or Glu101Gln. Studies with wild-type nikD show that formation of an ES complex with P2C partially overlaps with the onset of enzyme reduction (9). The initial lag observed when the reaction is monitored at 456 nm arises because the absorbance decrease due to enzyme reduction is counterbalanced by an absorbance increase in this region due to ES complex formation. This feature is apparent in the difference spectrum obtained for ES complex formation, as estimated by the spectral perturbation observed 0.74 ms after wild-type nikD is mixed with 2500 μ M P2C (Figure 9A,B, inset, black curve). The ES complex also exhibits a broad increase in absorption in the long-wave-

length region ($\lambda > 570$ nm) which is attributed to charge-transfer interaction between FAD and the electron-rich enamine tautomer of P2C (9). Although not detectable with unlabeled P2C, a time-dependent formation of the ES complex is observed in reductive half-reaction studies with wild-type nikD and [4,4,5,5,6,6- D_6]-P2C (9).

The spectral perturbation due to ES complex formation with Asp276Asn exhibits prominent positive bands at 464 and 492 nm and a weak negative band at 517 nm that are bathochromically shifted compared with the corresponding bands observed with wild-type nikD (442, 467, and 507 nm, respectively). The mutant complex also exhibits a broad increase in absorption at > 570 nm, similar to the wild-type complex, albeit considerably lower in intensity (Figure 9A, inset, red curve).

The difference spectrum obtained for the ES complex formed with Glu101Gln features a positive band at 477 nm with a pronounced shoulder at 455 nm and broad negative peaks at 525 and 365 nm (Figure 9B, inset, red curve) but does not exhibit an increase in absorbance within the accessible long-wavelength region ($\lambda \leq 700$ nm), unlike wild-type nikD. It is worth noting that a negative difference peak around 365 nm appears to be a signature motif of Glu101Gln complexes with active site ligands, as judged by results obtained with P2C, picolinate, CHA, and MeSeA ($\lambda_{\min} = 365, 361, 364, \text{ and } 361$ nm, respectively).

Spectral Course of the Reductive Half-Reaction with Asp276Asn or Glu101Gln with P2C. The reaction of Asp276Asn with various concentrations of P2C exhibits an apparently isosbestic loss of bands due to oxidized flavin at 456 and 378 nm (Figure 9A). Similar results are obtained with Glu101Gln except the isosbestic point is lost when the reaction is followed for longer times, accompanied by a very slow increase in absorbance at 456 nm (Figure 9B). The nature of this very slow spectral change is unclear. Reduction of both mutants is accompanied by a progressive loss of long-wavelength absorption, whereas a small transient increase in long-wavelength absorption is observed during reduction of wild-type nikD (9).

Kinetics of Binding of Picolinate to Glu101Gln. Unlike wild-type nikD or other mutants, a initial lag is not detected when reduction of Glu101Gln with P2C is monitored at 456 nm. We reasoned that an initial lag might not be detectable if the mutation accelerates the rate of ES complex formation. Evidence for evaluating this hypothesis was sought by determining the effect of the mutation on the rate of complex formation with picolinate. Studies with wild-type nikD show that picolinate binding is readily monitored by using a stopped-flow spectrometer. The observed rate of complex formation with the wild-type enzyme exhibits a linear dependence on ligand concentration with a finite y -intercept ($k_{\text{obs}} = k_1[L] + k_2$), as expected for a simple one-step approach to equilibrium ($K_d = k_2/k_1$) (9).

Binding of picolinate to Glu101Gln was assessed by monitoring the accompanying increase in absorbance at 480 nm. Reaction traces acquired over a 20-fold range of ligand concentrations exhibit monophasic kinetics ($y = Ae^{-kt} + B$), as illustrated by results obtained with 1500 μ M picolinate (Figure 10A). Unlike wild-type nikD, the observed rate of complex formation with Glu101Gln exhibits a hyperbolic dependence on picolinate concentration with a finite y -intercept (Figure 10B). This behavior is expected in the case of a two-step binding mechanism where formation of an initial complex is followed by an isomerization reaction to yield a more stable complex (25, 26) (Scheme 4). Fitting eq 4 to the data provides an estimated value of the

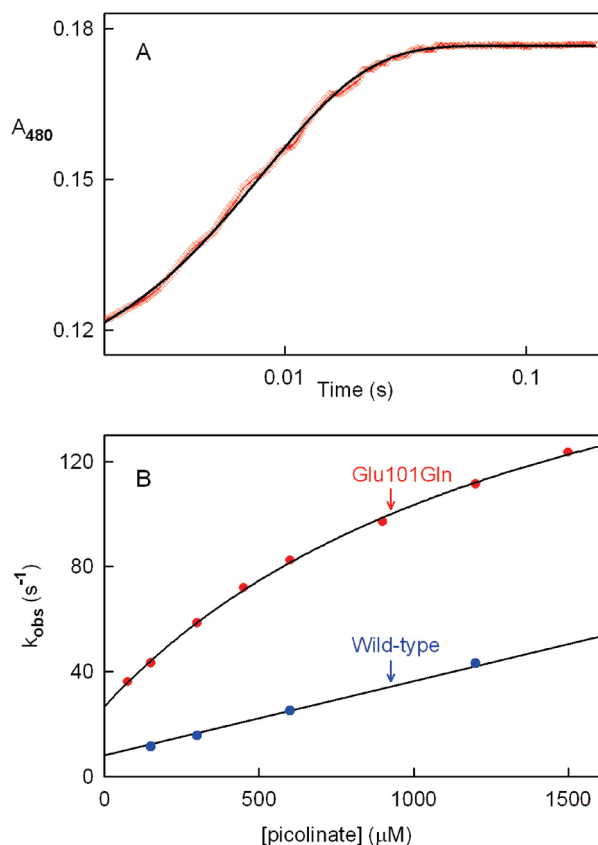
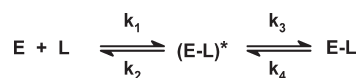


FIGURE 10: Kinetics of picolinate binding to Glu101Gln or wild-type nikD. Reactions were conducted in 100 mM potassium phosphate buffer (pH 8.0) at 25 °C. Complex formation was monitored at 480 nm using a stopped-flow spectrometer in photomultiplier mode. Panel A shows the reaction observed with Glu101Gln and 1500 μ M picolinate. The black line was obtained by fitting a single-exponential equation ($y = Ae^{-kt} + B$) to the data (red X's). Panel B shows the effect of picolinate concentration on the observed rate of complex formation. The black curve was obtained by fitting a hyperbola (eq 4) to data obtained with Glu101Gln (red circles). The black line was obtained by linear regression analysis of data obtained with wild-type nikD (blue circles). The wild-type nikD data were taken from ref 9.

Scheme 4: Two-Step Mechanism for Ligand Binding



microscopic K_d for the primary binding step (k_2/k_1) and rate constants for the reversible interconversion of the two complexes (k_3 and k_4) (Table 6).

$$k_{\text{obs}} = \frac{k_3[L]}{[L] + k_2/k_1} + k_4 \quad (4)$$

The overall macroscopic dissociation constant was calculated using these parameters and eq 5.

$$K_{d(\text{macroscopic})} = \frac{k_2 k_4}{k_1 k_3} \left(\frac{1}{1 + k_4/k_3} \right) \quad (5)$$

The calculated value ($K_d = 180 \pm 30 \mu\text{M}$) is, within experimental error, identical to the value obtained by spectral titration ($K_d = 151 \pm 2 \mu\text{M}$). Significantly, the observed rate of formation of a complex with Glu101Gln at a given picolinate concentration is 3–4-fold faster than the rate of the corresponding reaction with wild-type nikD (see Figure 10B). Assuming a similar enhanced

Table 6: Kinetics of Formation of a Complex with Picolinate and Glu101Gln or Wild-Type NikD^a

	Glu101Gln ^b	Wild-type ^c
k_1 ($\text{M}^{-1} \text{s}^{-1}$)	—	$(2.83 \pm 0.04) \times 10^4$
k_2 (s^{-1})	—	8.0 ± 0.7
k_2/k_1 (μM)	1500 ± 200	—
k_3 (s^{-1})	192 ± 9	—
k_4 (s^{-1})	27 ± 1	—
$K_{d(\text{macroscopic})}$ (μM)	180 ± 30 (calcd)	280 ± 30 (calcd)
	151 ± 2 (observed)	290 ± 40 (observed)

^a Reactions were conducted in 100 mM potassium phosphate buffer (pH 8.0) at 25 °C. ^b Values for k_2/k_1 , k_3 , and k_4 were determined by fitting eq 4 to the observed rate of complex formation at different picolinate concentrations. The value for the macroscopic K_d was calculated using eq 5, as described in the text. ^c Data previously reported (9). The calculated macroscopic K_d equals k_2/k_1 .

rate of ES complex formation and taking into account the ~4-fold slower rate of P2C oxidation to DHP, we estimate that mutation of Glu101 to Gln increases the kinetic resolution of binding and redox steps ~10-fold. This difference may be sufficient to account for the absence of a lag in the Glu101Gln reductive half-reaction.

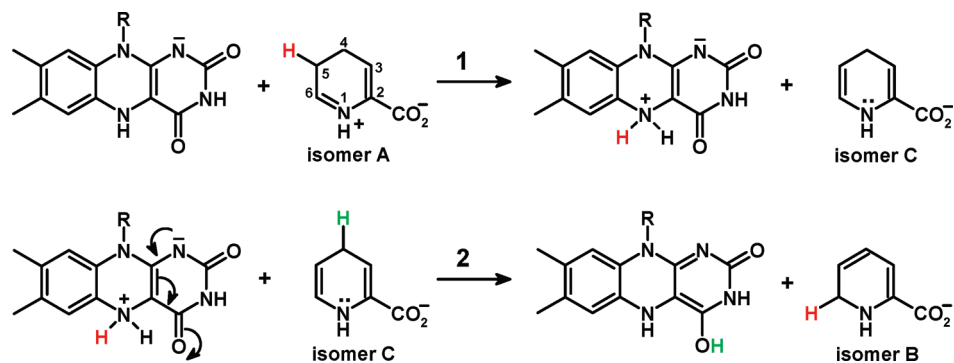
DISCUSSION

NikD catalyzes a remarkable aromatization reaction, involving two redox cycles, that converts P2C to picolinate, a key component of the nonribosomal peptide moiety in nikkomycin antibiotics. Stopped-flow studies of the reductive half-reaction with wild-type nikD showed that the enzyme oxidizes the enamine tautomer of P2C (9) but did not distinguish among several possible paths for the initial two-electron oxidation step (Scheme 2). In this study, we show that replacement of Glu101 or Asp276 with a neutral residue causes only a modest decrease (<5-fold) in the observed rate of oxidation of P2C to DHP. The results rule out the only possible candidates for a catalytic base in the initial two-electron oxidation step. This outcome provides compelling evidence that nikD oxidizes the bond between N(1) and C(6) in the enamine tautomer of P2C (Scheme 2, path A), ruling out alternative paths that require an active site base to mediate the oxidation of a carbon–carbon bond (Scheme 2, path B or C).

NikD exhibits a FAD–Trp355 charge-transfer band at weakly alkaline pH that is abolished upon protonation of an unknown ionizable residue that exhibits a pK_a of 7.3 in the wild-type enzyme (4). The loss of the charge-transfer band may reflect a pH-induced change from a coplanar to a perpendicular configuration of the flavin and indole rings, as observed in the open and closed crystal forms, respectively, of the nikD·picolinate complex (10). Protonation of the unknown residue is required for ligand binding, as judged by the observed effect of pH on the stability of enzyme·inhibitor complexes.² On the basis of its observed proximity, we hypothesized that the conformation of the Trp355 side chain might be affected by the protonation state of Glu101 or Asp276. However, substitution of Glu101 or Asp276 with a neutral amino acid does not eliminate the ionizable group, although the pK_a observed with the mutant enzymes is 1 or 2 pH units higher, respectively, compared with that of wild-type nikD. Mutagenesis studies that target more distal residues are currently in progress.

²R. C. Bruckner and M. S. Jorns, unpublished results.

Scheme 5: Postulated Role of Reduced Flavin as an Acid–Base Catalyst in the Isomerization of DHP



Although the critical redox step is only minimally effected, the Glu101Gln mutation results in an apparent change in the steady-state kinetic mechanism, as judged by the parallel line double-reciprocal plots observed under conditions (pH 8.0) where the wild-type enzyme or Asp276Asn exhibits an intersecting line pattern. The parallel line pattern indicates that an irreversible step occurs prior to reaction of the reduced mutant enzyme with oxygen. This criterion might be satisfied by an irreversible oxidation of P2C to DHP (Scheme 3, $k_{-2} = 0$) or by dissociation of the reduced enzyme·DHP complex. The second alternative is unlikely because studies with wild-type *nikD* show that the free reduced enzyme is not a kinetically competent intermediate.³ An intersecting line pattern clearly requires a reversible oxidation of P2C to DHP. However, the observed rate of reduction of wild-type *nikD* or either mutant at pH 8.0 exhibits a hyperbolic dependence on P2C concentration [$k_{\text{obs}} = k_{\text{lim}}[\text{P2C}]/(K_{\text{d app}} + [\text{P2C}])$], indicating that the oxidation step is practically irreversible (25). Interestingly, although an intersecting line pattern is observed with wild-type *nikD* at pH ≥ 8.0 , parallel line double-reciprocal plots are obtained at lower pH values.⁴ Overall, the results suggest that the steady-state kinetics observed with Glu101Gln do not reflect a fundamental mechanistic difference compared with wild-type enzyme.

The observed rate of formation of the Glu101Gln·picolinate complex exhibits a hyperbolic dependence on ligand concentration, indicative of a two-step binding mechanism in which an initial unstable complex, (E-L)*, is produced and then converted to a more stable species (Scheme 4). Interestingly, the crystal structures of the open and closed forms of the picolinate complex with wild-type *nikD* led us to propose a two-step binding mechanism. In this model, ligands were thought to form an initial open complex with the indole ring of Trp355 parallel to the flavin ring, followed by displacement of Trp355 to produce a more stable complex with ligand stacked above the flavin ring (17). However, the observed rate of complex formation with the wild-type enzyme was found to exhibit a linear dependence on picolinate concentration, consistent with a simple one-step approach to equilibrium (9). On the other hand, it should be noted that the results obtained with wild-type *nikD* do not rule out a limiting case of a two-step mechanism in which apparently linear kinetics are observed because the dissociation constant of the (E-L)* complex greatly exceeds the tested range of ligand concentrations. It is thus conceivable that the Glu101 mutation

may unmask the true binding mechanism by somehow increasing the stability of the (E-L)* complex.

Concluding Remarks. The studies described in this paper rule out Glu101 and Asp276, the only possible candidates for a catalytic base at the active site of *nikD*. The results not only provide compelling evidence regarding the nature of the initial two-electron oxidation step but also place an important constraint on the possible mechanism of DHP oxidation. Namely, picolinate formation must be accomplished by a pathway that does not involve oxidation of a carbon–carbon bond. This constraint prohibits further oxidation of DHP isomer A, the intermediate produced in the initial two-electron oxidation step, but is compatible with the oxidation of DHP isomer B (see Scheme 2). Importantly, the slow phase of the reductive half-reaction observed with wild-type *nikD* and [4,4,5,5,6,6- D_6]-P2C exhibits a kinetic isotope effect, indicating that this phase must involve cleavage of one or more C–H bonds in DHP isomer A (9).

DHP isomer A can be converted to DHP isomer B via a two-step isomerization reaction, as previously noted (9). We postulate that the 1,5-dihydroflavin anion (FADH^-) in the reduced enzyme·DHP complex acts as the acid–base catalyst required for DHP isomerization (Scheme 5). Significantly, the N(5) position in FADH^- is close to the C(5) and C(6) positions in DHP (3.66 and 3.41 Å, respectively), and the C(4)O position in FADH^- is near C(4) in DHP (3.77 Å), as judged by the structure of the closed *nikD*·picolinate complex (10). Conversion of DHP isomer A to DHP isomer C (Scheme 5, step 1) requires abstraction of a proton from the C(5)H group in isomer A and is likely to exhibit a pK_a of ~ 8 , as judged by the value obtained for the analogous ionization of P2C ($\text{pK}_a = 8.2$) (7, 8). We propose that the N(5)H group in FADH^- ($\text{pK}_a > 4$) (27) acts as the proton acceptor in this step. Isomerization of isomer C (Scheme 5, step 2) requires a proton donor at C(6) and a proton acceptor at C(4). We propose that the proton donor and acceptor functions are performed by N(5) H_2^+ and C(4)O groups in FADH^- , respectively. The postulated role of FADH^- as an acid–base catalyst in DHP isomerization is similar to that recently proposed for the reduced flavin cofactor in type 2 isopentenyl-diphosphate isomerase (28). To the best of our knowledge, *nikD* may provide the first example in which the impressive versatility of the flavin cofactor as a redox and an acid–base catalyst has been harnessed to accomplish a remarkable aromatization reaction.

ACKNOWLEDGMENT

We are grateful to Dr. Louis Silks (National Stable Isotope Resource at Los Alamos) for his generous gift of methylselenoacetate.

³P. R. Kommoju, R. C. Bruckner, and M. S. Jorns, unpublished results.⁴R. C. Bruckner and M. S. Jorns, unpublished results.

SUPPORTING INFORMATION AVAILABLE

Spectral properties of complexes formed with Glu101Gln or Asp276Asn and methylselenoacetate (Figure S1), steady-state kinetic analysis of P2C oxidation by Asp276Asn (Figure S2), and steady-state kinetic analysis of P2C oxidation by Glu101Gln (Figure S3). This material is available free of charge via the Internet at <http://pubs.acs.org>.

REFERENCES

- Lauer, B., Russwurm, R., Schwarz, W., Kalmanczhelyi, A., Bruntner, C., Rosemeier, A., and Bormann, C. (2001) Molecular characterization of co-transcribed genes from *Streptomyces tendae* Tu901 involved in the biosynthesis of the peptidyl moiety and assembly of the peptidyl nucleoside antibiotic nikkomycin. *Mol. Gen. Genet.* 264, 662–673.
- Hector, R. F. (1993) Compounds active against cell walls of medically important fungi. *Clin. Microbiol. Rev.* 6, 1–21.
- Bruntner, C., and Bormann, C. (1998) The *Streptomyces tendae* Tu901 L-lysine 2-aminotransferase catalyzes the initial reaction in nikkomycin D biosynthesis. *Eur. J. Biochem.* 254, 347–355.
- Venci, D., Zhao, G., and Jorns, M. S. (2002) Molecular characterization of nikD, a new flavoenzyme important in the biosynthesis of nikkomycin antibiotics. *Biochemistry* 41, 15795–15802.
- Bruckner, R. C., Zhao, G., Venci, D., and Jorns, M. S. (2004) Nikkomycin biosynthesis: Formation of a 4-electron oxidation product during turnover of nikD with its physiological substrate. *Biochemistry* 43, 9160–9167.
- Macholan, L., and Svatek, E. (1960) Aminoketocarbonsäuren VL: Über die konstitution und strukturformen der α -keto-analoga natürlicher diaminosäuren. *Collect. Czech. Chem. Commun.* 25, 2564–2575.
- Srinivasan, R., and Fisher, H. F. (1986) Structural features facilitating the glutamate dehydrogenase catalyzed α -imino acid- α -amino acid interconversion. *Arch. Biochem. Biophys.* 246, 743–750.
- Jorns, M. S., Bruckner, R. C., Zhao, G., Carrell, C. J., and Mathews, F. S. (2005) NikD: Crystal structures, charge transfer complex and endogenous ligands. In *Flavins and Flavoproteins 2005* (Nishino, T., Miura, R., Tanokura, M., and Fukui, K., Eds.) pp 773–785, ARchiTech Inc., Tokyo.
- Bruckner, R. C., and Jorns, M. S. (2009) Spectral and kinetic characterization of intermediates in the aromatization reaction catalyzed by nikD, an unusual amino acid oxidase. *Biochemistry* 48, 4455–4465.
- Carrell, C. J., Bruckner, R. C., Venci, D., Zhao, G., Jorns, M. S., and Mathews, F. S. (2007) NikD, an unusual amino acid oxidase essential for nikkomycin biosynthesis: Structures of closed and open forms at 1.15 and 1.90 Å resolution. *Structure* 15, 928–941.
- Khanna, P., and Jorns, M. S. (2001) Characterization of the FAD-containing N-methyltryptophan oxidase from *Escherichia coli*. *Biochemistry* 40, 1441–1450.
- Wu, X. L., Takahashi, M., Chen, S. G., and Monnier, V. M. (2000) Cloning of amadoriase I isoenzyme from *Aspergillus sp.*: Evidence of FAD covalently linked to Cys342. *Biochemistry* 39, 1515–1521.
- Miura, S., Ferri, S., Tsugawa, W., Kiin, S., and Sode, K. (2006) Active site analysis of fructosyl amine oxidase using homology modeling and site-directed mutagenesis. *Biotechnol. Lett.* 28, 1895–1900.
- Dodt, G., Kim, D. G., Reimann, S. A., Reuber, B. E., McCabe, K., Gould, S. J., and Mihalik, S. J. (2000) L-Pipecolic acid oxidase, a human enzyme essential for the degradation of L-pipecolic acid, is most similar to the monomeric sarcosine oxidases. *Biochem. J.* 345, 487–494.
- Wagner, M. A., Khanna, P., and Jorns, M. S. (1999) Structure of the flavocoenzyme of two homologous amine oxidases: Monomeric sarcosine oxidase and N-methyltryptophan oxidase. *Biochemistry* 38, 5588–5595.
- Trickey, P., Wagner, M. A., Jorns, M. S., and Mathews, F. S. (1999) Monomeric sarcosine oxidase: Structure of a covalently-flavinylated secondary amine oxidizing enzyme. *Structure* 7, 331–345.
- Bruckner, R. C., Zhao, G., Ferreira, P., and Jorns, M. S. (2007) A mobile tryptophan is the intrinsic charge transfer donor in a flavoenzyme essential for nikkomycin antibiotic biosynthesis. *Biochemistry* 46, 819–827.
- Palfey, B. A., and Massey, V. (1998) Flavin-dependent enzymes. In *Comprehensive Biological Catalysis* (Sinnott, M., Ed.) pp 83–154, Academic Press, New York.
- Fitzpatrick, P. F. (2007) Insights into the mechanisms of flavoprotein oxidases from kinetic isotope effects. *J. Labelled Compd. Radiopharm.* 50, 1016–1025.
- Silverman, R. B. (2000) The organic chemistry of enzyme-catalyzed reactions, Academic Press, San Diego.
- Zhao, G., Song, H., Chen, Z., Mathews, F. S., and Jorns, M. S. (2002) Monomeric sarcosine oxidase: Role of histidine 269 in catalysis. *Biochemistry* 41, 9751–9764.
- Ho, S. N., Hunt, H. D., Horton, R. M., Pullen, J. K., and Pease, L. R. (1989) Site-directed mutagenesis by overlap extension using the polymerase chain reaction. *Gene* 77, 51–59.
- Zhao, G., and Jorns, M. S. (2006) Spectral and kinetic characterization of the Michaelis charge transfer complex in monomeric sarcosine oxidase. *Biochemistry* 45, 5985–5992.
- Massey, V., and Ganther, H. (1965) On the interpretation of the absorption spectra of flavoproteins with special reference to D-amino acid oxidase. *Biochemistry* 4, 1161–1173.
- Strickland, S., Palmer, G., and Massey, V. (1975) Determination of dissociation constants and specific rate constants of enzyme-substrate (or protein-ligand) interactions from rapid reaction kinetic data. *J. Biol. Chem.* 250, 4048–4052.
- Chaiyen, P., Brissette, P., Ballou, D. P., and Massey, V. (1997) Thermodynamics and reduction kinetics properties of 2-methyl-3-hydroxypyridine-5-carboxylic acid oxygenase. *Biochemistry* 36, 2612–2621.
- Macheroux, P., Ghisla, S., Sanner, C., Rüterjans, H., and Müller, F. (2005) Reduced flavin: NMR investigation of N(5)-H exchange mechanism, estimation of ionisation constants and assessment of properties as biological catalyst. *BMC Biochem.* 6, 26–35.
- Unno, H., Yamashita, S., Ikeda, Y., Sekiguchi, S., Yoshida, N., Yoshimura, T., Kusunoki, M., Nakayama, T., Nishino, T., and Hemmi, H. (2009) New role of flavin as a general acid-base catalyst with no redox function in type 2 isopentenyl-diphosphate isomerase. *J. Biol. Chem.* 284, 9160–9167.